Experimental Neurology 286 (2016) 40–49

Contents lists available at ScienceDirect

Experimental Neurology

journal homepage: www.elsevier.com/locate/yexnr

Research Paper

HSPB3 protein is expressed in motoneurons and induces their survival after lesion-induced degeneration

Veronica La Padula [a,*], Ori Staszewski [b], Sigrun Nestel [c], Hauke Busch [d,e,f], Melanie Boerries [d,e,f], Eleni Roussa [a,c], Marco Prinz [b,g], Kerstin Krieglstein [a]

[a] Institute of Anatomy and Cell Biology, Department of Molecular Embryology, Albertstraße 17, 79104 Freiburg, Germany
[b] Institute of Neuropathology, Neurozentrum, Breisacherstraße 64, 79106 Freiburg, Germany
[c] Institute of Anatomy and Cell Biology, Department of Neuroanatomy, Albertstraße 17, 79104 Freiburg, Germany
[d] Systems Biology of the Cellular Microenvironment Group, Institute of Molecular Medicine and Cell Research, University of Freiburg, Germany
[e] German Cancer Consortium (DKTK), Freiburg, Germany
[f] German Cancer Research Center (DKFZ), Heidelberg, Germany
[g] BIOSS Centre for Biological Signalling Studies, University of Freiburg, Germany

ARTICLE INFO

Article history:
Received 2 March 2016
Received in revised form 8 July 2016
Accepted 23 August 2016
Available online 24 August 2016

Keywords:
Motoneuron
Chicken embryo
In ovo electroporation
Lesion-induced cell death
Small heat shock proteins
Charcot-Marie-Tooth disease
Distal hereditary motor neuropathy

ABSTRACT

The human small heat shock proteins (HSPBs) form a family of molecular chaperones comprising ten members (HSPB1–HSPB10), whose functions span from protein quality control to cytoskeletal dynamics and cell death control. Mutations in HSPBs can lead to human disease and particularly point mutations in HSPB1 and HSPB8 are known to lead to peripheral neuropathies. Recently, a missense mutation (R7S) in yet another member of this family, HSPB3, was found to cause an axonal motor neuropathy (distal hereditary motor neuropathy type 2C, dHMN2C).

Until now, HSPB3 protein localization and function in motoneurons (MNs) have not yet been characterized. Therefore, we studied the endogenous HSPB3 protein distribution in the spinal cords of chicken and mouse embryos and in the postnatal nervous system (central and peripheral) of chicken, mouse and human. We further investigated the impact of wild-type and mutated HSPB3 on MN cell death *via* overexpressing these genes *in ovo* in an avian model of MN degeneration, the limb-bud removal. Altogether, our findings represent a first step for a better understanding of the cellular and molecular mechanisms leading to dHMN2C.

1. Introduction

Charcot-Marie-Tooth (CMT) disease represent one of the most diffuse inherited disorder of the peripheral nervous system (PNS) diseases, with a frequency of 1 case in 2500 individuals. The demyelinating (CMT1) and axonal (CMT2) disease forms are distinguished according to the primarily affected cell types, the Schwann cells or the neurons, respectively (Patzko and Shy, 2011). So far, mutations in >40 genes have been identified in different forms of CMT (Tazir et al., 2014). Gene mutations resulting in axonal - CMT2 - pathogenesis cause alterations in structural proteins (*e.g.* neurofilament light chain, NF-L), proteins involved in mitochondrial function (*e.g.* mitofusin2, MFN2; ganglioside induced differentiation associated protein 1, GDAP1), intracellular protein dynamics (*e.g.* dynamin2, DNM2), apoptosis (*e.g.* small heat shock protein 1, HSPB1) or stress response (*e.g.* HSPB1 and small heat shock protein 8, HSPB8) (see El-Abassi et al., 2014 for a detailed review on CMT-related mutations). In addition to this classification, distal hereditary motor neuropathies (dHMN) comprise a group of hereditary diseases affecting the peripheral and slightly the sensory motor system. Their main and shared feature is the length-dependent motor neuropathy. Many genes have been identified to be causative for dHMN. They are involved in many functional aspects of the cellular physiology, such as protein misfolding (HSPB1, HSPB8), axonal transport (HSPB1; dynactin subunit 1, DNCT1) and RNA metabolism (senataxin, SETX; glycyl tRNA syntetase, GARS) (see Rossor et al., 2012 for a detailed review on dHMN-related genes).

The human HSPB family comprises 10 members (HSPB1-HSPB10) functioning mainly as molecular chaperones (Basha et al., 2012) and being also involved in cell death (Acunzo et al., 2012) and cytoskeletal dynamics (Wettstein et al., 2012). HSPBs are small ubiquitous

Abbreviations: MN, motoneuron; PNS, peripheral nervous system; CMT, Charcot-Marie-Tooth; dHMN, distal hereditary motor neuropathy; HSPB, small heat shock protein; IOE, *in ovo* electroporation; LBR, limb-bud removal.

* Corresponding author at: Institute of Anatomy and Cell Biology, Department of Molecular Embryology, 79104 Freiburg, Germany.
E-mail addresses: veronicalapadula@gmail.com (V. La Padula), ori.staszewski@uniklinik-freiburg.de (O. Staszewski), h.busch@dkfz.de (H. Busch), m.boerries@dkfz-heidelberg.de (M. Boerries), eleni.roussa@anat.uni-freiburg.de (E. Roussa), marco.prinz@uniklinik-freiburg.de (M. Prinz), kerstin.krieglstein@uniklinik-freiburg.de (K. Krieglstein).

http://dx.doi.org/10.1016/j.expneurol.2016.08.014

molecules, characterized by the presence of an alpha-crystallin domain, having a molecular weight ranging from 17 to 30 kDa and a length between 150 and 262 amino acids.

Recently, it was found that a heterozygous missense mutation (R7S) in the HSPB3 gene, the smallest member of the HSPB family, causes an early onset axonal motor neuropathy with mild or no sensory loss, classified as dHMN2C (Kolb et al., 2010). This pathogenic mutation is located in a highly conserved arginine residue at the N-terminal domain of the HSPB3 protein (Supplementary Fig. 1a, light grey box).

Mutations in five members of the HSPB family (HSPB1, HSPB3, HSPB4, HSPB5, and HSPB8) are linked to neurological and muscular diseases in humans. In particular, mutations on HSPB1 (Evgrafov et al., 2004; Houlden et al., 2008) (CMT2F and dHMN2B), HSPB8 (Irobi et al., 2010; Tang et al., 2005; Timmerman et al., 1996) (CMT2L and dHMN2A) and HSPB3 (Kolb et al., 2010) (dHMN2C) lead to peripheral neuropathies, but the mechanisms leading to CMT/dHMN have been characterized in detail for the former two, only, whereas nothing is currently known about the role of HSPB3 in dHMN2C.

While HSPB3 protein distribution has not yet been investigated, Northern blot and *in situ* hybridization (ISH) showed high mRNA levels in the heart and in smooth muscle (Sugiyama et al., 2000), yet low expression in the brain cortex and other cerebral areas (Kondaurova et al., 2011; Molyneaux et al., 2009). Still, ISH on the spinal cord of adult mice detected a low expression of HSPB3 in motoneurons (MNs) (Allen Spinal Cord Atlas, http://mousespinal.brain-map.org/). Additionally, RT-qPCR found a low expression of HSPB3 in the cerebellum, the spinal cord and the sciatic nerve (Kirbach and Golenhofen, 2011).

To follow up on these results we determined the localization of HSPB3 protein in the spinal cord and nerves of chicken, mouse, and human *via* optical, confocal, and transmission electron microscopy. Our histological findings prompted us to further investigate the HSPB3 function.

To do so, we used a paradigm of lesion-induced MN cell death, the limb-bud removal (LBR), combined with *in ovo* (meaning *in vivo* inside the egg) electroporation (IOE) technique on chicken embryos (La Padula et al., 2015) overexpressing the wild-type (WT) and mutated (R7S) HSPB3 on a plasmid in MNs undergoing cell death. In parallel, we overexpressed WT and mutated HSPB3 in embryos without LBR as control and because this experimental condition is closer to the pathological conditions in humans.

Altogether, our results indicate that HSPB3 plays an important role in MNs survival and that its pathogenic mutation in humans probably acquires a gain-of-function phenotype interfering with the normal activity of the endogenous wild type HSPB3 protein.

2. Materials and methods

2.1. Testing the primary antibody against HSPB3

The polyclonal antibody against HSPB3, made using a synthetic peptide based on the fragment 11–25 of the human HSPB3 protein (Supplementary Fig., 1a dark grey box), was purchased from Sigma-Aldrich (SAB1100972). The company reports its efficiency only on human-derived samples and does not mention any other specificity on different species. The homology between the human, avian, and murine 11–25 fragment sequence is very good (Supplementary Fig. 1b). The fragment 11–25 of the avian HSPB3 protein is not present in any other avian HSPB, and the same is valid for both the human and the murine fragments. We therefore exclude any unspecific staining of other HSPBs in our samples. We tested the antibody on Neuro2A cells (a murine neuroblastoma cell line) transfected or not with the plasmid carrying the wild type HSPB3 avian gene (Supplementary Fig. 1c) and stained against HSPB3 to detect the endogenous (murine) or the overexpressed (avian) HSPB3 protein in this *in vitro* model (Supplementary Fig. 1e-1 and e-2, respectively) following standard protocols. By pre-embedding immuno-electron microscopy (IEM) we detected HSPB3 in the cytoplasm of untransfected wild type Neuro2A cells (Supplementary Fig. 1e-1, arrows) and HSPB3 positivity is more evident in HSPB3-transfected Neuro2A (Supplementary Fig. 1e-2, arrows). To this positive control, we included negative controls omitting the primary and secondary antibodies (both in IEM and in immunohistochemistry) on chicken and human samples (Supplementary Fig. 1g-5 and g-8, Supplementary Fig. 2f and j for immunohistochemistry negative control stainings) where any positivity was detectable. We also added additional stainings on transversal sections of human muscle embedded in OCT compound (TissueTek, Thermo Fisher Scientific Inc.) for cryosectioning (muscular biopsies from patients that presented minor myopathic changes) (10 μm thick) using the following antibodies: anti-dystrophin (rod domain) 1 (anti-Dys1) (1:30, mouse monoconal, NCL-DYS1, clone Dy4/6D3, Novo Castra), anti-HSPB3 (1:50, rabbit polyclonal, SAB1100972, Sigma-Aldrich), anti-HSPB2 (1:50, mouse monoclonal, F-9 sc514154, Santa Cruz Biotechnology) (Supplementary Fig. 2).

We also transfected HeLa cells with our constructs and extracted the proteins to compare the HSPB3 expression of transfected cells (expressing the avian HSPB3 in its wild type and mutated forms) against negative (not transfected and expressing the empty plasmid) and positive (human muscle) controls (see further in "Protein extraction and Dot blots") (Supplementary Fig. 1f).

2.2. Histology and immunostainings

To study the HSPB3 protein distribution during avian development, chicken embryos (fertilized eggs of White Leghorn, *Gallus gallus domesticus*, were obtained from a local farm, Produits agricoles Haas, Kaltenhouse, France) were collected at different time points, from embryonic day (E) 3 (Hamburger and Hamilton, HH, stage 16–17) until E14 (HH40). Embryos were removed from the eggs, decapitated, eviscerated and immediately fixed by immersion in 4% paraformaldehyde (PFA) in 0.1 M phosphate buffer saline (PBS) pH 7.4 overnight (ON) at 4 °C. For E9, E12 and E14 embryos, legs and ribs were removed for better fixation and embedding. Samples were washed several times in 0.1 M PBS pH 7.4, incubated in 10% sucrose in 0.1 M PBS pH 7.4 on a rocking plate 6 h at room temperature (RT), submerged in 30% sucrose in 0.1 M PBS pH 7.4 ON at 4 °C and finally embedded in OCT compound (TissueTek, Thermo Fisher Scientific Inc.). Samples were stored at −20 °C until usage. Serial transverse sections (10–30 μm) of the spinal cord were cut with a Leica microtome (CM1520) (Leica Microsystems) and collected on superfrost slides (Mänzel-Gläser, Thermo Fisher Scientific Inc.). The mouse embryos (E13, kind gift of Dr. Vogel, University of Freiburg) followed the same fixation and embedding procedure. For motoneuron quantification, E6 chicken embryos followed the same embedding protocol (in the dark to preserve the GFP signal) and spinal cord transversal serial sections (10 μm) were cut from the tail over the lumbar part of the spinal cord. Postnatal chicken (2-years-old, kind gift of Haas farmer) and mouse (3-year-old female, kind gift of Dr. Vogel, University of Freiburg) samples were embedded in paraffin following standard protocols. Human samples (paraffin embedded, 4 μm) (the spinal cord is autoptic material, from a 64-year-old man and the sural nerve is a biopsy from a 50-year-old man) were obtained from the Institute of Neuropathology of Freiburg (Dr. Prinz, University of Freiburg) as well as the human muscular biopsies (gastrocnemius muscle from a 46-year-old man; cryosections, 10 μm). For immunofluorescence staining (Fig. 1 and Supplementary Fig. 1g), standard protocols (La Padula et al., 2015) were applied and the following primary antibodies were used: anti-Isl1/2 (39.4D5, 1:50), anti-vimentin (3CB2, 1:50), anti-nestin (RC2, 1:50), anti-neurofilament (4H6, 1:50) (all mouse monoclonal antibodies from Developmental Studies Hybridoma Bank), and the rabbit polyclonal anti-HSPB3 (SAB 1100972, 1:50, Sigma Aldrich). The appropriate secondary antibodies (goat anti-mouse AlexaFluor 568 and goat anti-rabbit AlexaFluor 488, Life Technologies) were applied 2 h at RT. Paraffin-embedded samples (Fig. 2), after deparaffination and quenching of the endogenous peroxidases,

followed the same staining protocol. The signal was enhanced with the ABC kit and revealed by diaminobenzidine (DAB) (Vectorlabs Inc.), sections were counterstained with hematoxylin, dehydrated and mounted with non-aqueous mounting medium (Entellan, Millipore).

The cryosections from muscle biopsies (Supplementary Fig. 2) were left to air dry, postfixed 30 min with 4% PFA in 0.1 M PBS, primary antibodies (anti-HSPB2 1:50, Santa Cruz Biotechnologies; anti-HSPB3, 1:50, Sigma Aldrich; anti-Dys1 1:30, Novo Castra) were diluted in 0.1 M PBS pH 7.4 and applied 2 h at RT. Slides were rinsed with 0.1 M PBS pH 7.4 and the appropriate secondary antibodies (donkey anti-rabbit Alexa Fluor 568 1:100; donkey anti-mouse Alexa Fluor 488 1:100, Life Technologies) diluted in 0.1 M PBS pH 7.4 were applied 1 h at RT. After rinsing in 0.1 M PBS pH 7.4, the slides were mounted with DAPI Fluoromount-G (Southern Biotech), let to air dry ON at RT in the dark and then stored at 4 °C.

Representative images of examined samples (20×) and of developmental HSPB3 distribution (20, 40, and 63×) were obtained with a Leica SP8 confocal microscope. For MN quantification, images were taken with a Nikon Axioplan 2 epifluorescence microscope at 40× magnification (see "Quantification and Statistics" for details). All the images in Supplementary Fig. 2 and Supplementary Fig. 1g have been acquired with a Leica SP8 confocal microscope at 63× magnification.

2.3. Gene cloning

The full length *Gallus gallus* (Gg) *domesticus* HSPB3 mRNA sequence (XM_001231557.1) was cloned in the pCIG vector (pCAGGS-IRES2-nucEGFP; Megason and McMahon, 2002) between the *Xho*I and *Eco*RI restriction sites. The cDNA was obtained pulling 10 spinal cords from E7 chicken embryos following standard protocols. Briefly, the spinal cords were homogenized by pottering and the total RNA was extracted using TriFast (PeqLab) and bromo-chloro-propane. The HSPB3 insert was obtained by PCR amplification (GgHSPB3-F 5′-ACCCTCGAGATGGC AGAAGCTGTTATAAG-3′; GgHSPB3-R 5′-ACCGAATTCCTAATTAATTCC CACCGAG-3′) and purified from a 1% agarose gel using the Nucleo Spin Gel and PCR cleanup kit (Macherey-Nagel GmbH). The HSPB3 product was sequenced and then inserted into the pCIG vector using standard ligation protocols.

The HSPB3-R7S insert was obtained using the gene synthesis service provided by GenScript.

2.4. Limb-bud removal combined with in ovo electroporation (LBR/IOE)

Fertilized eggs from White Leghorn chickens (*Gallus gallus domesticus*) were obtained from a local farm (Produits agricoles Haas, Kaltenhouse, France) and then incubated in a humidified incubator at 38 °C on their long side. Embryos were staged accordingly to the Hamburger and Hamilton (HH) classification (Hamburger and Hamilton, 1951). Eggs were windowed and HH16–17 embryos were selected for limb-bud removal (LBR) followed by *in ovo* electroporation (IOE) as previously described (La Padula et al., 2015). The empty pCIG vector, the pCIG-HSPB3-WT or the pCIG-HSPB3-R7S plasmids (5–7 μg/μL) were used for IOE. After electroporation, the embryos were rinsed with sterile 0.1 M PBS pH 7.4, sealed and reincubated to reach the sixth embryonic day (E6).

2.5. Quantification and statistics

Isl1/2 positive cells were manually counted with the multi-point tool of ImageJ software. We counted every 10th section (25 sections average per sample) on the electroporation side with or without LBR and on the contralateral side without lesion as an internal control. Then, the percentage of the surviving MNs was calculated normalizing the data on the control side. Three independent samples were quantified for every condition. Significance was calculated by unpaired *t*-test. Results are expressed as the average percentage ± SEM.

2.6. Bioinformatic analysis

The sequences of HSPB3 human, mouse and avian proteins (NP_006299.1, NP_064344.1, XP_001231558.1) were compared by using the multiple alignment tool of ClustalW2 (http://www.ebi.ac.uk/Tools/msa/clustalw2/) using default settings.

For mRNA (NM_006308.2, NM_019960.2, XM_001231557.2) and protein comparisons of the human, murine and avian HSPB3 and the other HSPBs, the algorithms blastn/discontinuous blast and BlastP were used with default settings.

2.7. Cell culture

Neuro2A cells (Sigma-Aldrich) were cultured on 12 mm round glass coverslips placed in a 24-well plate in presence of DMEM supplemented with 4.5% glucose, 1% penicillin/streptomycin, 1% of non-essential amino acids (NEAA) and 10% fetal bovine serum (FBS) (all components were purchased from Life Technologies). Cells at 60–70% of confluency were transfected with the pCIG-HSPB3-WT construct using Lipofectamine (Sigma-Aldrich) following manufacturer's instructions. The day after, the GFP signal was checked at an inverted fluorescence microscope (Axio Imager 2, Zeiss), and cells were fixed for electron microscopy.

HeLa cells (Sigma-Aldrich) were cultured on 6-well plates in presence of DMEM supplemented with 10% FBS and 1% penicillin/streptomycin/neomycin (PSN) (Life Technologies). Like for the Neuro2A cells, HeLa cells were transfected when the 60–70% of confluency was reached, with the empty pCIG plasmid, the pCIG-HSPB3-WT, the pCIG-HSPB3-R7S constructs using Lipofectamine (Sigma-Aldrich) following manufacturer's instructions (untransfected cells followed the same protocol omitting the plasmid at the plasmid incubation step). The day after, the GFP signal was checked, and cells were harvested for the following protein extraction.

2.8. Pre-embedding immuno-electron microscopy

The culture medium was removed from the Neuro2A cell cultures, cells were washed 2 times with sterile 0.1 M PBS and then fixed with 4% PFA plus 0.1% (final concentration) glutaraldehyde (GA) in 0.1 M phosphate buffer (PB) pH 7.4 for 1 h at RT. Cells were washed three times in 0.1 M PB, washed with 50 mM Tris buffered saline (TBS), and the epitopes blocked adding 20% normal goat serum (NGS) 1 h at RT. Primary antibody against HSPB3 (Sigma-Aldrich) was diluted (1:50) in 50 mM TBS with 2% NGS, added on the coverslips, and incubated ON at 4 °C. The day after, coverslips were washed with 50 mM TBS and the secondary biotinylated goat anti-rabbit antibody (1:100) (Linaris Biologische Produkte GmbH) diluted in 50 mM TBS with 2% NGS was applied on the cells and incubated ON at 4 °C. Finally, cells were washed with 50 mM TBS, and the avidin-biotin conjugated peroxidase complex (ABC) was applied 1 h at RT. The DAB reaction was developed and observed against a white background (4 min of development). The reaction was stopped with TBS and the cells were washed in 50 mM TBS 15 min. Cells were then postfixed in 1% osmium tetroxide in 0.1 M PB with 6.85% sucrose 1 h at RT, rinsed, and serially dehydrated in graded ethanols to be embedded in Durcupan resin (Electron Microscopy Sciences) using the flat embedding configuration. The same protocol was used for silver-enhancement staining, where a secondary gold-conjugated (8 nm) antibody was used. Ultrathin (60–70 nm) sections were cut with a 45° diamond knife (Diatome) at a Leica ultracut EM UC7 (Leica Microsystems) and collected on formvar-carbon-coated nickel grids (Electron Microscopy Sciences). Images were taken with a LEO 906E electron microscope at 100 kV using a 2K CCD camera "sharp eye" (Tröndle).

2.9. Post-embedding immuno-electron microscopy

The spinal cord dissected from E7 chicken embryos were fixed with 4% PFA plus 0.1% (final concentration) GA diluted in 0.1 M PB pH 7.4 ON at 4 °C. The day after, samples were rinsed several times in 0.1 M PB pH 7.4 and then dehydrated with an ascending ethanol scale at RT in agitation, pre-impregnated in London Resin White (LRW) (Electron Microscopy Sciences) resin in a 1:1 ratio in absolute ethanol 1 h 30' at 4 °C in agitation and then impregnated in pure LRW ON at 4 °C on a rocking plate. Finally, another step with fresh LRW was added (1 h at 4 °C on rocking plate), samples were transferred in gelatin capsules filled with fresh LRW, let 1 h RT to settle and finally placed at 55 °C two days for complete resin polymerization. Ultrathin (60–70 nm) sections were cut with a 45° diamond knife (Diatome) at a Leica ultracut EM UC7 (Leica Microsystems) and collected on formvar-carbon-coated nickel grids (Electron Microscopy Sciences). Images were taken with a LEO 906E electron microscope at 100 kV using a 2 K CCD camera "sharp eye" (Tröndle).

2.10. Cryo-electron microscopy and immuno-electron microscopy

The spinal cord and the sciatic nerves were dissected from a *P*32 mouse (a kind gift of Dr. Frick, University of Bordeaux) perfused with 4% PFA in 0.1 M PB pH 7.4 and postfixed in 4% PFA plus 0.2% GA (final concentration) ON at 4 °C. The day after, the samples were rinsed with 0.1 M PB pH 7.4, washed twice in 50 mM glycine in 0.1 M PB pH 7.4, and then placed in 2.3 M sucrose in 0.1 M PB pH 7.4 ON at 4 °C on a rocking plate. The samples were put on OCT compound (TissueTek, Thermo Fisher Scientific Inc.) and cut using a cryoultramicrotome Leica UC7-FC7 (Leica Microsystems) at −120 °C and an immuno-diamond knife (Diatome). Ultrathin sections (60–70 nm) were picked-up with a mixture of 2% methylcellulose/2.3 M sucrose (v/v), collected on formvar-carbon-coated nickel grids (Electron Microscopy Sciences) and immunostained using standard protocols. Briefly, sections were treated with 50 mM glycine for aldehyde quenching, epitopes were blocked with 0.1 M PBS/1% BSA, incubated with the primary antibody anti-HSPB3 (1:70) (Sigma-Aldrich, SAB1100972), washed, and then the reaction was revealed using a goat anti-mouse gold-conjugated (10 nm) secondary antibody (1:50) (Aurion). Images were taken on a TEM Hitachi H7650 at 80 kV.

2.11. Protein extraction and Dot blots

HeLa cells were harvested in 150 μL of NP40 cell lysis buffer (Thermofisher Scientific) supplemented with protease and phosphatase inhibitors (Sigma-Aldrich). The cells were scraped off the Petri dish with sterile cell scrapers (Sigma Aldrich). The lysates were collected in sterile tubes and kept at −20 °C until usage.

Unfixed cryosections from human muscle biopsies were obtained from the Department of Neuropathology, University of Freiburg. Isolation of proteins from muscle tissue cryosections was performed using the Qproteome FFPE Tissue Kit from Qiagen (Hilden, Germany) according to the manufacturer's instructions. Dot blots were performed essentially as described earlier (Roussa et al., 2008). 80 mg protein of HeLa cells either non transfected (C), transfected with empty vector (P), transfected with HSPB3 (H) or transfected with mutant HSPB3 (R), and 20 mg of protein obtained from human muscle biopsies (M) was loaded onto nitrocellulose membrane. The membrane was blocked with 3% low fat milk powder in TTBS (Tris-Tween-buffered-saline) and incubated with primary anti-HSPB3 (1:1000), anti-GFP (1:1000), anti-GAPDH (1:10,000) or anti-Dys-1 (1:500) overnight at 4 °C. The following day the membrane was incubated with either anti-mouse or anti-rabbit IgG coupled to peroxidase (1:10,000) and was developed using the Cell Signaling SignalFire© enhanced chemiluminescence (ECL) detection system. Signals were visualized on X-ray film.

3. Results

3.1. HSPB3 protein distribution

3.1.1. HSPB3 protein distribution in the chicken (E3–E14) and mouse (E13) embryos

To elucidate the HSPB3 protein localization, we stained coronal spinal cord sections of chicken embryos during development from the embryonic developmental day three (E3) until E14, when the developmental programmed cell death (PCD) of MNs ends (Hamburger and Hamilton stages HH16–17 till HH40) (Hamburger and Hamilton, 1951). HSPB3 (green; Fig. 1a–i) was detectable in the radial glia (RG) (vimentin, red; Fig. 1a–c) starting from E3 (inset in Fig. 1a, arrows) until E12 (Fig. 1e, arrows) when its expression decreased concomitantly with RG differentiation (McDermott et al., 2005), persisting in the remaining RG until E14 (not shown). Interestingly, we found the same distribution in the RG in the spinal cord of E13 (corresponding to the chicken embryonic day 6) mouse embryos (nestin, red; Fig. 1f), suggesting a conserved distribution pattern among species. On the contrary, MNs somata (Isl1/2, red; Fig. 1a'–c') did not appear HSPB3-positive before E7 (Fig. 1c', arrowheads), becoming detectable at E9 (Fig. 1d, arrowheads) and being evident at E12 (Fig. 1e, arrowheads). Interestingly, HSPB3 appeared in MN axons as early as E4 (neurofilaments, red; Fig. 1g, arrows), when MNs start elongating their axons to the periphery, and persisted in PNS axons till E14 (Fig. 1i). At E6, HSPB3 was detectable in the axons of both motor (Fig. 1h, arrow) and sensory (Fig. 1h, arrowhead) neurons as well. Additionally, the dermomyotome, the tissue precursor of the skeletal muscle (von Maltzahn et al., 2012), appeared to be strongly positive in the chicken embryo (Fig. 1a and a', E3, asterisks; Fig. 1g, E4, asterisk).

3.1.2. HSPB3 protein expression in postnatal chicken, mouse and human

The first symptoms of dHMN2C due to the HSPB3-R7S mutation begin in the second decade of a patients' life. Therefore we tested, whether HSPB3 expression was still present in MNs postnatally, and whether HSPB3 protein was distributed in the PNS as well. For this, we compared both longitudinally cut peripheral nerves (Fig. 2a–c) and transversally cut spinal cords (Fig. 2d–f) from different vertebrates, namely adult chicken (Fig. 2a and d), mouse (Fig. 2b and e), and human (Fig. 2c and f). One of the more interesting features we found was that HSPB3 protein is localized in the axons of both PNS motor (Fig. 2a and b, arrows, chicken and mouse sciatic nerves) and PNS sensory (Fig. 2c, arrows, human sural nerve biopsy) neurons. Indeed, it is well known that other HSPB members, such as HSPB1, HSPB5 and HSPB8, interact with cytoskeletal proteins. It has been demonstrated that HSPB1 plays a role in the regulation of axonal transport by decreasing tubulin acetylation and consequently causing the destabilization of the microtubule network (d'Ydewalle et al., 2011). Several HSPB1 mutations causing CMT2F/dHMN2B have been identified (see Datskevich et al., 2012 for a review). Similarly, HSPB8 mutations have the same influence on the axonal stability but the way HSPB8 interacts with the microtubules is still not known. Presumably, this could happen through its association with HSPB1 (Fontaine et al., 2005). Regarding HSPB5, mutations of this protein can cause myofibrillary myopathy (Sacconi et al., 2012) and it has been demonstrated that HSPB5 acts as a chaperone for actin and desmin (Perng et al., 1999).

In the spinal cord, HSPB3 was found perinuclearly in MNs (Fig. 2d–f, arrows) as well as in glial cell cytoplasm (Fig. 2d–f, arrowheads). Localization of HSPB3 in the motor and sensory systems was further confirmed by staining in the axons of both the ventral and dorsal roots of the mouse spinal cord (Fig. 2g and h, arrows) and in dorsal root ganglia (DRG) somata (Fig. 2l, arrowhead). The distribution in DRGs was already present in E14 chicken embryos (Fig. 2i, arrowhead).

Taken together, our data confirmed the presence of HSPB3 protein in both motor and sensory neurons, which suggests a putative

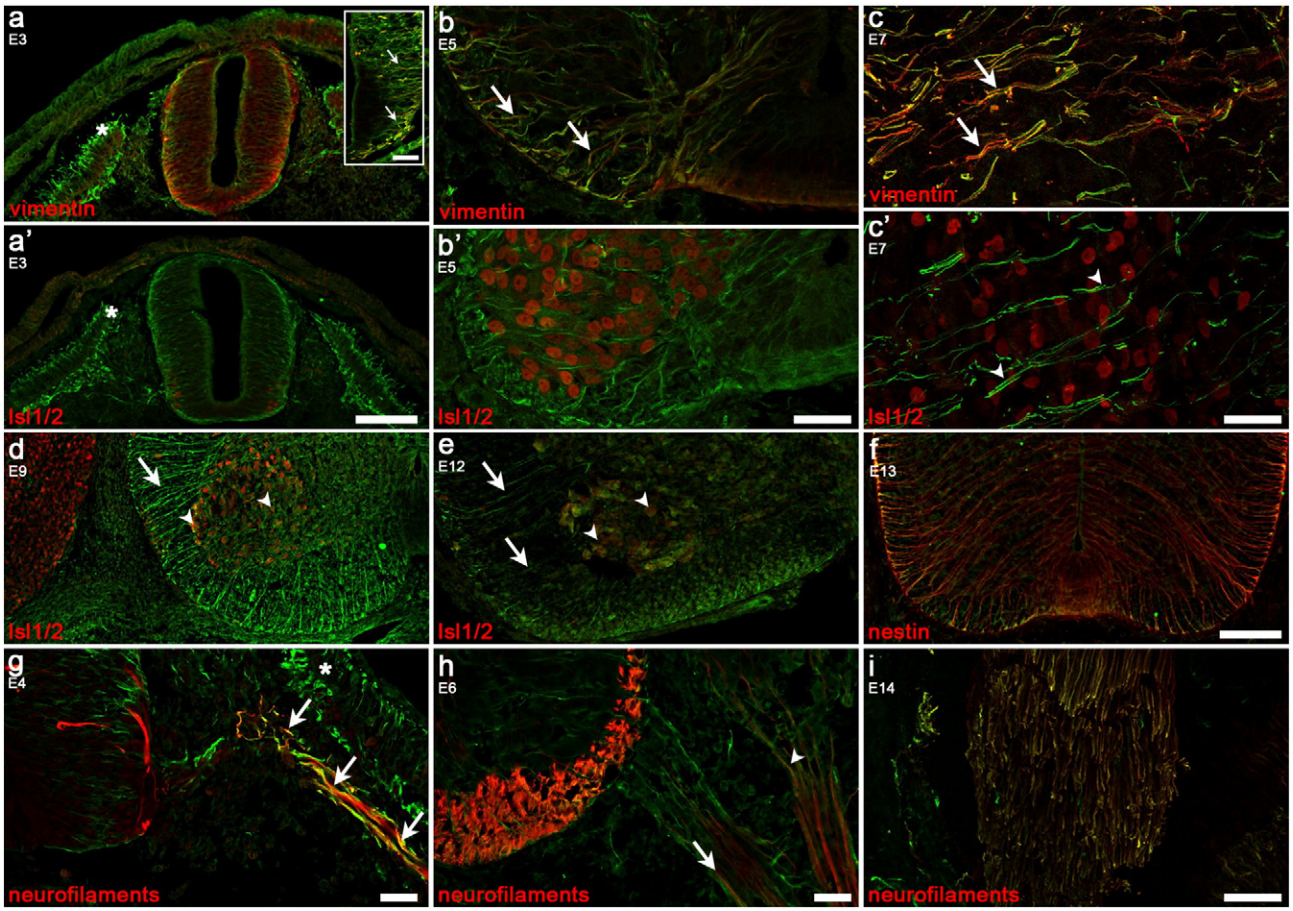

Fig. 1. HSPB3 protein distribution during chicken embryonic development and in E13 mouse embryos: (a–i) HSPB3 protein (green) is expressed throughout the chicken embryonic development, from embryonic day 3 (E3, a and a') till E14 (i). (a–e) From E3 (a, arrows) till E12 (e, arrowhead) HSPB3 is expressed in radial glia (RG) (vimentin, red; a–c and inset in a, arrows). (g–i) HSPB3 is also localized in the axons (neurofilament, red) of motor (g and h, arrows; E4 and E6) and sensory (h, arrowhead; E6) neurons and later in the axons of peripheral nerves (i, E14). (a, a' and g) The dermomyotome clearly express HSPB3 (asterisks; E3 and E4). (a'–c', d and e) Cell bodies of MNs (red, Isl1/2) start being positive for HSPB3 protein from E9 (d, arrowheads) till E12 (e, arrowheads). (f) In mouse embryos (E13), HSPB3 is expressed in RG (nestin, red) as well. Scale bars: a-a' and d–f (20× magnification), 100 μm; b–b', c–c', i (63× magnification) and g–h (40× magnification), 25 μm.

role in the neuronal development and homeostasis, justifying its role in the motor neuropathy with a mild sensory loss as described in those patients carrying the R7S mutation of HSPB3 (Kolb et al., 2010).

3.1.3. Subcellular distribution of HSPB3

Having determined the cell-type specific distribution of HSPB3, we next sought to elucidate its subcellular localization by immuno-electron microscopy (IEM) both *in vitro* and *in vivo*. A pre-embedding

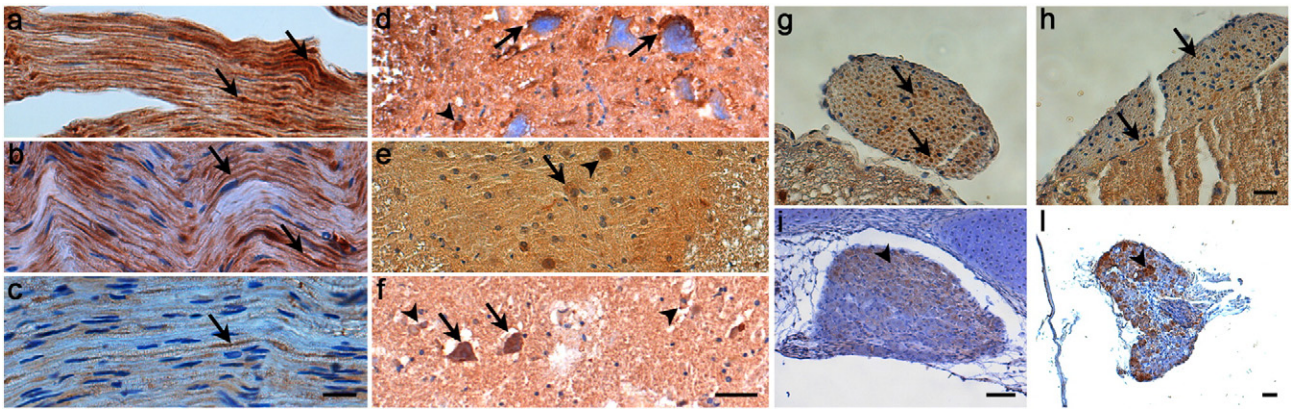

Fig. 2. HSPB3 protein distribution in spinal cord and peripheral nerve of postnatal chicken, mouse and human: (d–f) Postnatally, HSPB3 localizes perinuclearly in spinal cord MNs (arrows), in the glial cytoplasm (arrowheads), and (a–c) in the axons of peripheral nerves (arrows) in adult chicken (a and d), mouse (b and e), and human (c and f). (g–h and l) It can be found in the axons of both the ventral (h) and dorsal (g) roots of spinal cord and in the dorsal root ganglia (DRG) (l) of the adult mouse. (i) Its expression is already present in the chicken embryo DRG at E14. Scale bars: a–c, g, h, 20 μm; d–f, i, l, 50 μm.

IEM against HSPB3 on untransfected Neuro2A cells (a murine neuroblastoma cell line) detected endogenous HSPB3 protein in various cellular compartments, such as the cytoplasm (Fig. 3a–d, asterisks), actin filaments (Fig. 3a–c, arrows), the outer mitochondrial membrane (OMM) (Fig. 3a, c and d, black arrowheads) and to some extent in mitochondrial cristae (Fig. 3d, white arrowhead). Since the scarce localization in the cristae could be attributed to the limitations of the pre-embedding IEM, we employed more sensitive post-embedding labeling procedures for the following experiments.

We stained coronal sections of spinal cords from postnatal mice (*P*32, Fig. 3e and f) and chicken embryos (E7, Fig. 3 h) as well as longitudinal sections of the murine sciatic nerve (Fig. 3g) to investigate the ultrastructural expression of HSPB3 in the CNS and the PNS. We found that HSPB3 has a similar distribution *in vivo* and *in vitro*, being present in MN cytoplasm (Fig. 3f, asterisk), and in neurofilaments in the axons of both central (Fig. 3e,f,h and inset in Fig. 3h, arrows) and peripheral (Fig. 3g, arrows) nervous systems. At the mitochondrial level, HSPB3 positivity is not only restricted to the OMM (Fig. 3e,g and h, black arrowheads) and cristae (Fig. 3e,g and h, white arrowheads), but is also found in the inner mitochondrial membrane (IMM) (Fig. 3e and f, dark grey arrowheads). Of note, the cytoplasmic and cytoskeletal distribution of HSPB3 was visible by all microscopy methods (Fig. 1d–e and g–i; Fig. 2), whereas the mitochondrial localization was only detectable due to the higher sensitivity of the electron microscopy.

3.2. Overexpression of HSPB3-WT and HSPB3-R7S in the chicken embryo subjected or not to limb-bud removal

To evaluate the roles of WT HSPB3 and of its R7S mutated form on MNs survival, we cloned the chicken HSPB3 gene (WT or R7S) in a pCIG (pCAGGS-IRES2-nucEGFP) overexpression vector (Megason and McMahon, 2002) (Supplementary Fig. 1c) using an empty pCIG vector as an internal control. Plasmids were transferred into the neural tube of E3 chicken embryos (Supplementary Fig. 1d-1 and d-2) by *in ovo* electroporation (IOE) using a diagonal configuration of the electrodes to better target the MN progenitors, as previously described (La Padula et al., 2015) (Supplementary Fig. 1d-3). Transfected embryos were sacrificed three days later - at E6 - before the start of the developmental PCD period at E6.5–E7. Quantifying the effect of WT and mutated HSPB3 at E6 was important, since PCD not only reduces the number of MNs but also modifies their gene expression. To compare the effect of HSPB3-WT and R7S on healthy and on dying MNs, we established two experimental conditions: the first consisted in electroporating the spinal MNs by IOE on normal embryos and the second involved an additional LBR (schematized in Supplementary Fig. 1d-4 and d-5 and in Fig. 4d and h).

3.2.1. Effects of the overexpressed HSPB3-WT and HSPB3-R7S on healthy and degenerating MNs

Overexpression of HSPB3-WT (Fig. 4b) significantly reduced the number of MNs in normal (without LBR) conditions compared to control (pCIG empty vector; Fig. 4a) (reduction of 20.53%: pCIG 92.03% ± 2.9 *vs.* WT 71.5% ± 1.4; $p = 0.0016$, Fig. 4d), whereas in conditions of cell degeneration with LBR HSPB3-WT (Fig. 4f) rescued a significant number of dying MNs compared to the pCIG control (Fig. 4e) (increase by 43.5%: pCIG 41.6% ± 15 *vs.* WT 85.2% ± 2.4; $p = 0.025$, Fig. 4h). Overexpression of HSPB3-R7S showed a higher variability in inducing MN survival or death compared to HSPB3-WT. Indeed, HSPB3-R7S (Fig. 4g) did not show a significant difference in the rescue of MNs after lesion compared to control (Fig. 4e) (increase by 35.9%: pCIG 41.6% ± 15 *vs.* R7S 77.6% ± 13.4; $p = 0.094$, Fig. 4h), although there was a mild trend in increased MN survival. On the contrary, HSPB3-R7S overexpression without lesion (Fig. 4c) had a pronounced effect on MN death compared to control (Fig. 4a) (decrease by 35.8%: pCIG 92.03% ± 2.9 *vs.* R7S 56.18% ± 9.1; $p = 0.01$, Fig. 4d). Importantly, there was no significant difference between the effects obtained by HSPB3-WT and HSPB3-R7S in both conditions (without LBR, difference by 15.31%, $p = 0.11$; with LBR, difference of 7.6%, $p = 0.53$).

Taken together, these results strongly indicate that HSPB3-WT and its mutation R7S share common properties on MNs survival and death, and that such properties depend on the cellular state.

4. Discussion

The family of small heat shock proteins (HSPBs) represents an important group of ubiquitous proteins involved in key processes of the cellular physiology, such as cell survival, cytoskeletal remodeling, and protein degradation. In humans, 10 members (HSPB1–10) have been

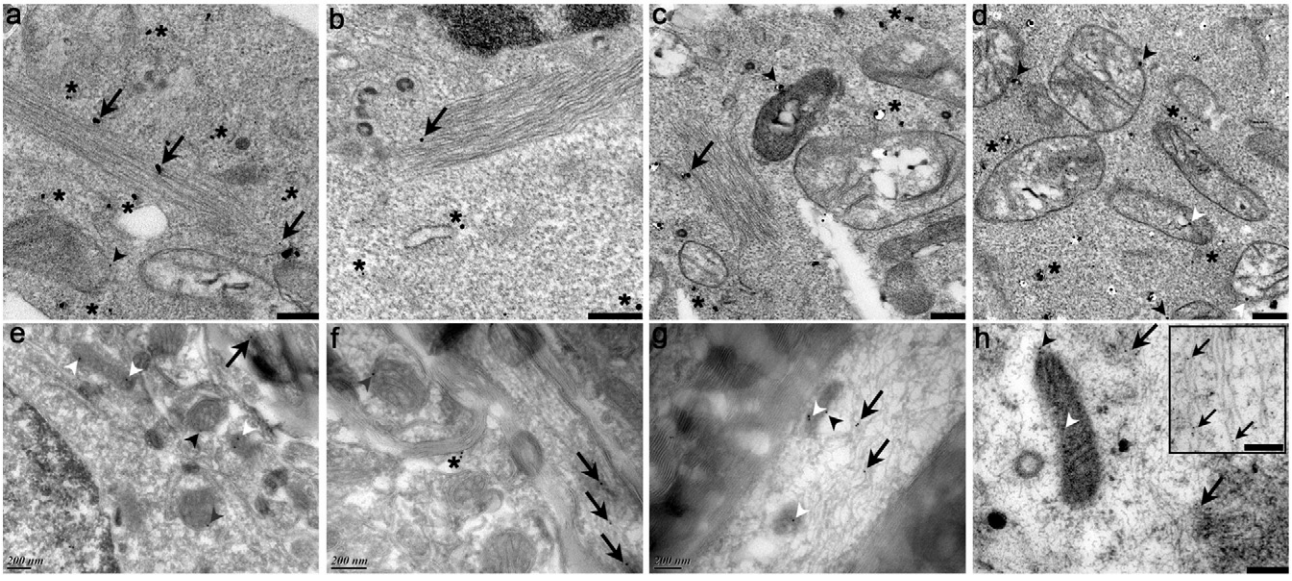

Fig. 3. Subcellular distribution of HSPB3 protein *in vitro* and *in vivo*: (a–d) *In vitro*, on Neuro2A cells, HSPB3 protein is diffusely distributed in the cytoplasm (a–d, asterisks). It is also localized in actin filament bundles (a–c, arrows) and at the level of the outer mitochondrial membrane (a, c, d, black arrowheads) and cristae (d, white arrow). (e–h) HSPB3 has a similar distribution *in vivo*, in postnatal (*P*32) mouse (spinal cord, e–f; sciatic nerve, g) and chicken embryo (E7) (spinal cord, h), being expressed in mitochondrial outer (e, g and h, black arrowheads) and inner (e and f, dark grey arrowheads) membranes and in cristae (e, g and h, white arrowheads), and neurofilaments in both central (e, f, h, inset in h) and peripheral (g) nervous systems (arrows). Magnification: a, c, d, 10K; b, 16.7K; e, 70K; f, 100K; g, 80K; h, 13K; inset in h, 16.7K Scale bars a–d, h and inset in h 250 nm; e–g, 200 nm.

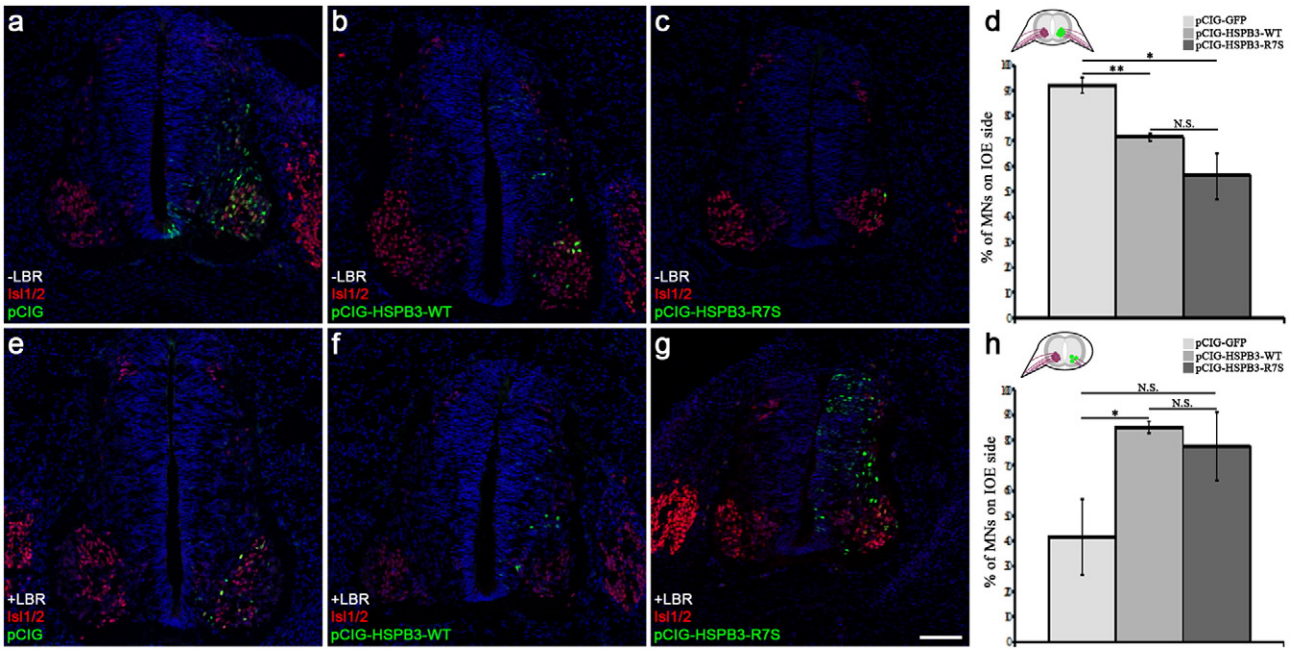

Fig. 4. The overexpression of HSPB3 in both its WT and mutated form induces motoneuron reduction or recovery depending on the cellular conditions: (a–d) the overexpression of HSPB3-WT (green; b) or of its mutated form R7S (green; c) causes a significant decrease (d) of MN (Isl1/2, red; a–c) number in E6 chicken embryos without limb-bud removal (LBR), whereas the overexpression of the empty plasmid pCIG (green; a) does not induce any change in the MN population number. (e–h) On the contrary, the overexpression of HSPB3-WT (green; f) induces a significant MN (Isl1/2, red; e–g) survival in E6 chicken embryos undergoing lesion-induced cell death due to LBR (h) while HSPB3-R7S overexpression (green; g) displays a tendency in the rescue, albeit not significant (h). The overexpression of the pCIG plasmid alone (e, green) does not cause any MN rescue and does not interfere with the cell death induced by the LBR. The schemas in d and h represent the experimental conditions. $n = 3$ from three independent experiments. Columns represent mean ± SEM. Scale bar, 50 μm.

identified, and mutations of many HSPBs have been related to human pathologies. Notably, three of them (HSPB1, HSPB3, and HSPB8) cause motor neuropathies.

In this work, we studied the distribution of HSPB3 in the nervous system of chicken, mouse and human by light, confocal and electron microscopy. We investigated its function on avian motoneuron (MN) survival using a paradigm of lesion-induced cell death (the limb-bud removal, LBR) (Oppenheim et al., 1978) combined with the electroporation *in ovo* (IOE) of HSPB3 wild type (WT) or of its mutation R7S on the developing chicken embryo. The two goals of our work consisted first in acquiring a better understanding on the localization of the endogenous HSPB3 and, second, in knowing the function and effects of HSPB3-WT and of its pathogenic mutated form (HSPB3-R7S) - which is known to cause a genetic peripheral neuropathy classified as dHMN2C (Kolb et al., 2010) - on healthy and degenerating MNs.

Structurally, HSPBs are characterized by the presence of an alpha-crystallin domain, the target of many of the mutations causing human diseases. Nonetheless, mutations involving the N′- or the C′-terminal domains of HSPBs are disease causing in humans. Among them is the R7S mutation that is located on the N′-terminal of the HSPB3 protein. Four different mutations have been documented on this domain in HSPB1, all causing distal hereditary motor neuropathies (Datskevich et al., 2012).

In this work, we showed for the first time the embryonic and postnatal localization of the HSPB3 protein in the central and peripheral nervous systems, finding it localized in the cytoplasm of glial cells as well as in the cell bodies and axons of motor and sensory neurons. Interestingly, HSPB3 localization in MNs changed over time, appearing diffused in the somata in late avian embryonic stages (not detectable until E9) and perinuclear postnatally (in all the species examined). We think that this shift is due to the different molecular processes occurring in MNs during development. Indeed, HSPB3 somatic localization appeared to be detectable by confocal microscopy only at E9 and much more at E12, when the developmental programmed cell death was reaching its end. The perinuclear distribution has been documented also in MNs of postnatal transgenic mice overexpressing the human HSPB1 (Sharp et al., 2006).

At the ultrastructural level, HSPB3 is widely distributed within the cell. Indeed, we found it located in the cytosol, associated to the outer and inner mitochondrial membranes (OMM and IMM), to mitochondrial cristae and also to actin bundles and neurofilaments *in vitro* and *in vivo*. These data are particularly interesting, because both mitochondrial and neurofilament dysfunctions are at the base of several types of peripheral neuropathies, such as CMT2E/1F (neurofilament light chain, NF-L) (Fabrizi et al., 2007), CMT2A (mitofusin, MFN2) (Stuppia et al., 2015) and CMT4A (ganglioside-induced differentiation-associated protein 1, GDAP1) (Niemann et al., 2005).

The translocation to the mitochondria has been shown for the phosphorylated form of HSPB5 in mouse retina under stress conditions using biochemical methods confirming its localization at mitochondrial cristae by immuno-electron microscopy (IEM) (Chis et al., 2012). Nonetheless, Nakagawa and colleagues showed by biochemical and immunolocalization studies that HSPB2 is loosely associated with the OMM (Nakagawa et al., 2001). Using a similar approach, Morrow and colleagues (Morrow et al., 2000), showed that the *Drosophila melanogaster* ortholog of HSPB8 (DmHsp22) is located in the mitochondrial matrix. The same group (Morrow et al., 2004), demonstrated that both the ubiquitous or MN-restricted overexpression of DmHsp22 extends the Drosophila life span and that the MN overexpression results in the maintenance of a normal locomotion pattern and in a higher resistance of MNs to oxidative stress. A shift to a mitochondrial localization has also been documented *in vitro* for HSPB1 on butyrate-treated IEC-18 cells, an intestinal crypt cell line (Parhar et al., 2006). In the light of these findings we propose that HSPB3 - similar to HSPB2, HSPB5, and HSPB1 - is a cytoplasmic protein able to dynamically translocate to mitochondria, where it putatively interacts with proteins

involved in cellular survival or death. Here, we showed the cytoskeletal localization of HSPB3 that is a feature shared with other small heat shock proteins (such as HSPB1 and HSPB5; Miron et al., 1991; Perng et al., 1999), which suggests that HSPB3 could play a role in cytoskeletal dynamics regulation as well. Indeed, it has been demonstrated that point mutations affecting HSPB1 and HSPB5 lead to axonal CMT and myofibrillary myopathy (Houlden et al., 2008; Sacconi et al., 2012) and that HSPB1 acts as a negative regulator of actin polymerization (Miron et al., 1991). Our finding justifies the axonal length-dependent motor neuropathy caused by the HSPB3-R7S point mutation in the affected subjects.

Finally, we studied the functional properties of HSPB3 on healthy and dying MNs, demonstrating that both the WT and the mutated HSPB3 proteins play a similar role on MNs survival and death. We overexpressed by IOE HSPB3-WT or its pathogenic mutation R7S in dying MNs of embryos presenting LBR. The quantification of the surviving MNs three days after the induction of degeneration showed that both HSPB3-WT and R7S were able to rescue MNs from cell death, albeit the latter less markedly than the former, and that they induced a similar cell loss when overexpressed in healthy MNs (without LBR). Based on our results, we conclude that HSPB3 plays a role in spinal MNs survival, when the apoptotic machinery is activated in both its WT and mutated form.

Many HSPBs - such as HSPB1, HSPB2, and HSPB8 - play a role on cell survival, directly acting on the main actors involved in cell death. Notably, the overexpression of HSPB1 following nerve crush in rats is able to rescue MNs from cell death (Benn et al., 2002). Indeed, the anti-apoptotic function of HSPB1 has been well documented, identifying its function as a negative modulator of apoptosis (Charette and Landry, 2000; Paul et al., 2010). Interestingly, a recent study on MDA-MB-231, a human breast cancer cell line, has identified the anti-apoptotic properties of HSPB2, inhibiting caspase-2 activation and Bid cleavage (Oshita et al., 2010). A wider effect on cell survival is exerted by HSPB8, which plays a role on both survival and apoptosis (Aurelian et al., 2012; Modem et al., 2011; Sharma et al., 2006; Smith et al., 2011) (see Table 1b for the function of HSPBs on cell death). We found such a dual role for HSPB3 as well. It is protective when overexpressed in degenerating MNs and inducing cellular loss if overexpressed in steady-state MNs, which is akin to the behavior of HSPB8. Given these facts together with our data we propose that HSPB3 exerts its function in the spinal cord preferentially by interacting with the more abundant HSPB8 rather than with HSPB2 (the low expression of HSPB2 mRNA has been shown in spinal cord MNs by the Allen Spinal Cord Atlas, http://mousespinal.brain-map.org/). For this reason, HSPB3 could putatively act as a cell death inhibitor or inductor according to the cellular background of gene expression in spinal cord MNs.

Very little is known about HSPB3 interaction partners. Notably, HSPB3 interaction with HSPB2 has been documented as important for the muscular development (Sugiyama et al., 2000), whereas the effect of its relation with HSPB8 is not known (Fontaine et al., 2005). It is important to note that HSPB8 interacts with HSPB1 and HSPB2 (Sun et al., 2004) (Table 1a) and that HSPB1 and HSPB8 proteins are expressed in MNs cell bodies (Crippa et al., 2010; Sharp et al., 2006). Therefore, we assume that a functional redundancy among the HSPBs would justify the low severity and the slow progression of the dHMN2C caused by the R7S mutation in HSPB3 alone. We also evaluated the interactions occurring among HSPBs and other relevant proteins by using the Human Integrated Protein-Protein Interaction rEference (HIPPIE), a database that applies a specific algorithm to assign a rate of protein-protein interaction (PPI) based on the quantity and the quality of scientific evidence for a given interaction (Schaefer et al., 2012) (Table 1a). All these interactions are considered of high confidence (confidence score > 0.73). Yet the PPI between HSPB3 and HSPB8 obtained a confidence score of 0.63, having been demonstrated by a high-throughput yeast two-hybrid technique alone (Table 1a) but we believe, based on our results, that further studies could confirm such interaction. Additionally, the interaction between HSPB3 and neurofilament light chain (NF-L) was shown by automated yeast two-hybrid analysis (score 0.63; Stelzl et al., 2005). This, as mentioned before, is confirmed by our IEM analysis. Moreover, mutations of the gene coding for NF-L induces cytoskeletal disorganization, causing an axonal form of CMT (CMT2E; Fabrizi et al., 2007).

Peripheral neuropathy in humans is caused by a heterozygous mutation in HSPB3. The symptoms start around the second life decade and the disease develops progressively over years, indicating a slow MN degeneration. In combination with our findings this suggests that the human HSPB3-R7S presents a gain-of-function, compensated in part by the presence of the endogenous HSPB3-WT protein in MNs. Based on the similar behavior between the WT and the mutated R7S protein, one could conclude that the mutated protein has no pathogenic effect. We think this is not the case and we believe that long-term *in vivo* studies in mouse are needed to provide necessary information on the function of this protein - in its WT and mutated forms -, which we showed to be important for MNs physiology. Indeed, our experimental conditions were not designed to extend the time window of HSPB3 overexpression, due to the fact that the ontogenetic programmed cell death taking place in MNs occurring in the embryo starting at E6.5–E7 would have reduced the MN population and modified their genetic background. Consequently, this wouldn't have allowed us evaluating the effects of HSPB3-WT and R7S on cell survival of MNs undergoing induced cell death in the living chicken embryo, the second aim of our study.

Whether the interaction of the HSPB3-R7S protein with its partners - like HSPB8, HSPB2, mitochondrial or neurofilament proteins - differs

Table 1
a. Relevant protein-protein interactions (PPI) performed by HSPB proteins. b. Activity of HSPB proteins on cell survival.

a.

	Interactor	HIPPIE PPI	Methods used to establish PPI	Reference
HSPB3	HSPB2	0.80	Affinity chromathography, affinity capture-western, *in vivo*	Sugiyama et al., 2000
	HSPB8	0.63	Two-hybrid screening	Fontaine et al., 2005
	NF-L	0.63	Two-hybrid screening	Stelzl et al., 2005
HSPB8	HSPB1	0.96	FRET, affinity capture-western, affinity chromathography, *in vitro*	Fontaine et al., 2005
	HSPB2	0.88	FRET, affinity capture-western, affinity chromathography, coimmunoprecipitation	Fontaine et al., 2005

b.

	Action on apoptosis	Way of action	Reference
HSPB1	Inhibition	Inhibition of: Cyt C, casp3, Daxx	Benn et al., 2002 Charette and Landry, 2000
HSPB2	Inhibition	Inhibition of: casp2, Bid cleavage	Oshita et al., 2010
HSPB8	Inhibition	Prevention or reduction of partially unfolded proteins	Chavez Zobel et al., 2003
	Induction	Interaction with protein kinases (*e.g.* ERK1/2); Bag3 interaction	Shemetov et al., 2011; Carra et al., 2008
HSPB3	Inhibition	Not known	Data presented in our work
	Induction	Not known	

compared to the WT protein is not known and would certainly be important to investigate.

Gain-of-function mutations have been documented for other proteins involved in the pathogenesis of peripheral neuropathies, leading to both axonal and demyelinating CMT (Grandis et al., 2008; Motley et al., 2011; Sowa et al., 2014).

In summary, our work shows that HSPB3 protein is distributed in the central and peripheral nervous systems, and that its overexpression in MNs undergoing cell death is able to rescue them from apoptosis, indicating its potential role as a modulator of MN survival. In addition, its pathogenic mutation R7S behaves in a similar way than the WT protein, suggesting a non-deleterious effect on the protein function but rather a modification of its behavior on the long-term, maybe by inducing the formation of protein aggregates and a following unfolded protein response in the spinal MNs, as shown in the case of HSPB1 (Ylikallio et al., 2015).

5. Conclusions

Taken together, our data justify the symptoms and the progression of the human pathology documented for the mutated HSPB3 protein, and open new perspectives for the study of therapeutic approaches.

Regarding long-term studies to perform on mice, it is actually important to note that knock-out mice for HSPB1 and HSPB5 do not mimic the phenotype of the pathology (Brady et al., 2001; Huang et al., 2007), but only transgenic mice carrying the pathogenic mutations do (Andley et al., 2011; Lee et al., 2015). For this reason, we think that the creation of a transgenic mouse carrying the HSPB3-R7S gene could better contribute to the understanding of the cellular and molecular mechanisms leading to the dHMN2C caused by the R7S mutation of HSPB3. In addition, such a model would allow therapeutic interventions for which we envision various different approaches: the first would be the selective inhibition of the mutated protein by RNA interference (RNAi), as it has already been successfully done *in vivo* in a mouse model of amyotrophic lateral sclerosis (Xia et al., 2006). The second would consist in the overexpression of the WT protein, in an attempt to rescue MNs from degeneration. And, lastly, one could combine these two strategies to improve the chances of rescuing MNs from an early degenerative state.

Another gene therapy option could be the overexpression of other HSPBs, direct or indirect interactors of HSPB3. This idea has been recently proven to be effective *in vitro* in the case of three HSPB5 pathogenic mutations (Hussein et al., 2015).

Alternatively, a pharmaceutical approach could be explored, like the inhibition *via* specific drugs of deacetylating enzymes, whose efficacy was demonstrated *in vivo* on mice carrying two different mutations of HSPB1 that induced CMT2F and dHMN2B; in these mice, the inhibition of the histone deacetylase 6 (HDAC6) enzyme rescued their phenotype (d'Ydewalle et al., 2011). Despite all these initial insights, an in depth understanding of the molecular pathways around HSPB3 will be necessary for a successful *in vivo* therapy in humans.

Supplementary data to this article can be found online at http://dx.doi.org/10.1016/j.expneurol.2016.08.014.

Acknowledgements

The Authors are grateful to the German Research Foundation (Deutsche Forschungsgemeinschaft, DFG) for the financial support (DFG; Kr1477/11-3) given to the project. We would like to thank Ms. Lidia Koschny, Ms. Ute Baur and Ms. Ellen Gimbl for their precious help for the histology, the molecular biology, and the cell culture experiments. We are also thankful to Dr. Amparo Tolosa for her guidance in the gene cloning process. The immuno-electron microscopy was done in the Bordeaux Imaging Center, a service unit of the CNRS-INSERM and Bordeaux University, member of the national infrastructure France BioImaging, and the help of Melina Petrel and Etienne Gontier is acknowledged. The Authors declare no competing financial interests.

References

Acunzo, J., Katsogiannou, M., Rocchi, P., 2012. Small heat shock proteins HSP27 (HSPB1), alphaB-crystallin (HSPB5) and HSP22 (HSPB8) as regulators of cell death. Int. J. Biochem. Cell Biol. 44, 1622–1631.

Andley, U.P., Hamilton, P.D., Ravi, N., Weihl, C.C., 2011. A knock-in mouse model for the R120G mutation of alphaB-crystallin recapitulates human hereditary myopathy and cataracts. PLoS One 6, e17671.

Aurelian, L., Laing, J.M., Lee, K.S., 2012. H11/HSPB8 and its herpes simplex virus type 2 homologue ICP10PK share functions that regulate cell life/death decisions and human disease. Autoimmune diseases 2012, 395329.

Basha, E., O'Neill, H., Vierling, E., 2012. Small heat shock proteins and alpha-crystallins: dynamic proteins with flexible functions. Trends Biochem. Sci. 37, 106–117.

Benn, S.C., Perrelet, D., Kato, A.C., Scholz, J., Decosterd, I., Mannion, R.J., Bakowska, J.C., Woolf, C.J., 2002. Hsp27 upregulation and phosphorylation is required for injured sensory and motor neuron survival. Neuron 36, 45–56.

Brady, J.P., Garland, D.L., Green, D.E., Tamm, E.R., Giblin, F.J., Wawrousek, E.F., 2001. AlphaB-crystallin in lens development and muscle integrity: a gene knockout approach. Invest. Ophthalmol. Vis. Sci. 42, 2924–2934.

Carra, S., Seguin, S.J., Lambert, H., Landry, J., 2008. HspB8 chaperone activity toward poly(Q)-containing proteins depends on its association with Bag3, a stimulator of macroautophagy. J. Biol. Chem. 283, 1437–1444.

Charette, S.J., Landry, J., 2000. The interaction of HSP27 with Daxx identifies a potential regulatory role of HSP27 in Fas-induced apoptosis. Ann. N. Y. Acad. Sci. 926, 126–131.

Chavez Zobel, A.T., Loranger, A., Marceau, N., Theriault, J.R., Lambert, H., Landry, J., 2003. Distinct chaperone mechanisms can delay the formation of aggresomes by the myopathy-causing R120G alphaB-crystallin mutant. Hum. Mol. Genet. 12, 1609–1620.

Chis, R., Sharma, P., Bousette, N., Miyake, T., Wilson, A., Backx, P.H., Gramolini, A.O., 2012. Alpha-crystallin B prevents apoptosis after H2O2 exposure in mouse neonatal cardiomyocytes. Am. J. Physiol. Heart Circ. Physiol. 303, H967–H978.

Crippa, V., Sau, D., Rusmini, P., Boncoraglio, A., Onesto, E., Bolzoni, E., Galbiati, M., Fontana, E., Marino, M., Carra, S., Bendotti, C., De Biasi, S., Poletti, A., 2010. The small heat shock protein B8 (HSPB8) promotes autophagic removal of misfolded proteins involved in amyotrophic lateral sclerosis (ALS). Hum. Mol. Genet. 19, 3440–3456.

Datskevich, P.N., Nefedova, V.V., Sudnitsyna, M.V., Gusev, N.B., 2012. Mutations of small heat shock proteins and human congenital diseases. Biokhimiya/Biochemistry 77, 1500–1514.

d'Ydewalle, C., Krishnan, J., Chiheb, D.M., Van Damme, P., Irobi, J., Kozikowski, A.P., Vanden Berghe, P., Timmerman, V., Robberecht, W., Van Den Bosch, L., 2011. HDAC6 inhibitors reverse axonal loss in a mouse model of mutant HSPB1-induced Charcot-Marie-Tooth disease. Nat. Med. 17, 968–974.

El-Abassi, R., England, J.D., Carter, G.T., 2014. Charcot-Marie-tooth disease: an overview of genotypes, phenotypes, and clinical management strategies. PM & R: the journal of injury, function, and rehabilitation 6, 342–355.

Evgrafov, O.V., Mersiyanova, I., Irobi, J., Van Den Bosch, L., Dierick, I., Leung, C.L., Schagina, O., Verpoorten, N., Van Impe, K., Fedotov, V., Dadali, E., Auer-Grumbach, M., Windpassinger, C., Wagner, K., Mitrovic, Z., Hilton-Jones, D., Talbot, K., Martin, J.J., Vasserman, N., Tverskaya, S., Polyakov, A., Liem, R.K., Gettemans, J., Robberecht, W., De Jonghe, P., Timmerman, V., 2004. Mutant small heat-shock protein 27 causes axonal Charcot-Marie-Tooth disease and distal hereditary motor neuropathy. Nat. Genet. 36, 602–606.

Fabrizi, G.M., Cavallaro, T., Angiari, C., Cabrini, I., Taioli, F., Malerba, G., Bertolasi, L., Rizzuto, N., 2007. Charcot-Marie-Tooth disease type 2E, a disorder of the cytoskeleton. Brain J. Neurol. 130, 394–403.

Fontaine, J.M., Sun, X., Benndorf, R., Welsh, M.J., 2005. Interactions of HSP22 (HSPB8) with HSP20, alpha B-crystallin, and HSPB3. Biochem. Biophys. Res. Commun. 337, 1006–1011.

Grandis, M., Vigo, T., Passalacqua, M., Jain, M., Scazzola, S., La Padula, V., Brucal, M., Benvenuto, F., Nobbio, L., Cadoni, A., Mancardi, G.L., Kamholz, J., Shy, M.E., Schenone, A., 2008. Different cellular and molecular mechanisms for early and late-onset myelin protein zero mutations. Hum. Mol. Genet. 17, 1877–1889.

Hamburger, V., Hamilton, H.L., 1951. A series of normal stages in the development of the chick embryo. J. Morphol. 88, 49–92.

Houlden, H., Laura, M., Wavrant-De Vrieze, F., Blake, J., Wood, N., Reilly, M.M., 2008. Mutations in the HSP27 (HSPB1) gene cause dominant, recessive, and sporadic distal HMN/CMT type 2. Neurology 71, 1660–1668.

Huang, L., Min, J.N., Masters, S., Mivechi, N.F., Moskophidis, D., 2007. Insights into function and regulation of small heat shock protein 25 (HSPB1) in a mouse model with targeted gene disruption. Genesis 45, 487–501.

Hussein, R.M., Benjamin, I.J., Kampinga, H.H., 2015. Rescue of alphaB crystallin (HSPB5) mutants associated protein aggregation by co-expression of HSPB5 partners. PLoS One 10, e0126761.

Irobi, J., Almeida-Souza, L., Asselbergh, B., De Winter, V., Goethals, S., Dierick, I., Krishnan, J., Timmermans, J.P., Robberecht, W., De Jonghe, P., Van Den Bosch, L., Janssens, S., Timmerman, V., 2010. Mutant HSPB8 causes motor neuron-specific neurite degeneration. Hum. Mol. Genet. 19, 3254–3265.

Kirbach, B.B., Golenhofen, N., 2011. Differential expression and induction of small heat shock proteins in rat brain and cultured hippocampal neurons. J. Neurosci. Res. 89, 162–175.

Kolb, S.J., Snyder, P.J., Poi, E.J., Renard, E.A., Bartlett, A., Gu, S., Sutton, S., Arnold, W.D., Freimer, M.L., Lawson, V.H., Kissel, J.T., Prior, T.W., 2010. Mutant small heat shock

protein B3 causes motor neuropathy: utility of a candidate gene approach. Neurology 74, 502–506.
Kondaurova, E.M., Naumenko, V.S., Sinyakova, N.A., Kulikov, A.V., 2011. Map3k1, Il6st, Gzmk, and HSPB3 gene coexpression network in the mechanism of freezing reaction in mice. J. Neurosci. Res. 89, 267–273.
La Padula, V., Koszinowski, S., Krieglstein, K., 2015. The combination of limb-bud removal and in ovo electroporation techniques: a new powerful method to study gene function in motoneurons undergoing lesion-induced cell death. J. Neurosci. Methods 239, 206–213.
Lee, J., Jung, S.C., Joo, J., Choi, Y.R., Moon, H.W., Kwak, G., Yeo, H.K., Lee, J.S., Ahn, H.J., Jung, N., Hwang, S., Rheey, J., Woo, S.Y., Kim, J.Y., Hong, Y.B., Choi, B.O., 2015. Overexpression of mutant HSP27 causes axonal neuropathy in mice. J. Biomed. Sci. 22, 43.
McDermott, K.W., Barry, D.S., McMahon, S.S., 2005. Role of radial glia in cytogenesis, patterning and boundary formation in the developing spinal cord. J. Anat. 207, 241–250.
Megason, S.G., McMahon, A.P., 2002. A mitogen gradient of dorsal midline Wnts organizes growth in the CNS. Development 129, 2087–2098.
Miron, T., Vancompernolle, K., Vandekerckhove, J., Wilchek, M., Geiger, B., 1991. A 25-kD inhibitor of actin polymerization is a low molecular mass heat shock protein. J. Cell Biol. 114, 255–261.
Modem, S., Chinnakannu, K., Bai, U., Reddy, G.P., Reddy, T.R., 2011. Hsp22 (HSPB8/H11) knockdown induces Sam68 expression and stimulates proliferation of glioblastoma cells. J. Cell. Physiol. 226, 2747–2751.
Molyneaux, B.J., Arlotta, P., Fame, R.M., MacDonald, J.L., MacQuarrie, K.L., Macklis, J.D., 2009. Novel subtype-specific genes identify distinct subpopulations of callosal projection neurons. J. Neurosci. Off. J. Soc. Neurosci. 29, 12343–12354.
Morrow, G., Inaguma, Y., Kato, K., Tanguay, R.M., 2000. The small heat shock protein Hsp22 of *Drosophila melanogaster* is a mitochondrial protein displaying oligomeric organization. J. Biol. Chem. 275, 31204–31210.
Morrow, G., Samson, M., Michaud, S., Tanguay, R.M., 2004. Overexpression of the small mitochondrial Hsp22 extends *Drosophila* life span and increases resistance to oxidative stress. FASEB J.: official publication of the Federation of American Societies for Experimental Biology 18, 598–599.
Motley, W.W., Seburn, K.L., Nawaz, M.H., Miers, K.E., Cheng, J., Antonellis, A., Green, E.D., Talbot, K., Yang, X.L., Fischbeck, K.H., Burgess, R.W., 2011. Charcot-Marie-Tooth-linked mutant GARS is toxic to peripheral neurons independent of wild-type GARS levels. PLoS Genet. 7, e1002399.
Nakagawa, M., Tsujimoto, N., Nakagawa, H., Iwaki, T., Fukumaki, Y., Iwaki, A., 2001. Association of HSPB2, a member of the small heat shock protein family, with mitochondria. Exp. Cell Res. 271, 161–168.
Niemann, A., Ruegg, M., La Padula, V., Schenone, A., Suter, U., 2005. Ganglioside-induced differentiation associated protein 1 is a regulator of the mitochondrial network: new implications for Charcot-Marie-Tooth disease. J. Cell Biol. 170, 1067–1078.
Oppenheim, R.W., Chu-Wang, I.W., Maderdrut, J.L., 1978. Cell death of motoneurons in the chick embryo spinal cord. III. The differentiation of motoneurons prior to their induced degeneration following limb-bud removal. J. Comp. Neurol. 177, 87–111.
Oshita, S.E., Chen, F., Kwan, T., Yehiely, F., Cryns, V.L., 2010. The small heat shock protein HSPB2 is a novel anti-apoptotic protein that inhibits apical caspase activation in the extrinsic apoptotic pathway. Breast Cancer Res. Treat. 124, 307–315.
Parhar, K., Baer, K.A., Parker, K., Ropeleski, M.J., 2006. Short-chain fatty acid mediated phosphorylation of heat shock protein 25: effects on camptothecin-induced apoptosis. Am. J. Physiol. Gastrointest. Liver Physiol. 291, G178–G188 (1069).
Patzko, A., Shy, M.E., 2011. Update on Charcot-Marie-Tooth disease. Curr. Neurol. Neurosci. Rep. 11, 78–88.
Paul, C., Simon, S., Gibert, B., Virot, S., Manero, F., Arrigo, A.P., 2010. Dynamic processes that reflect anti-apoptotic strategies set up by HSPB1 (Hsp27). Exp. Cell Res. 316, 1535–1552.
Perng, M.D., Cairns, L., van den, I.P., Prescott, A., Hutcheson, A.M., Quinlan, R.A., 1999. Intermediate filament interactions can be altered by HSP27 and alpha B-crystallin. J. Cell Sci. 112 (Pt 13), 2099–2112.
Rossor, A.M., Kalmar, B., Greensmith, L., Reilly, M.M., 2012. The distal hereditary motor neuropathies. J. Neurol. Neurosurg. Psychiatry 83, 6–14.
Roussa, E., Oehlke, O., Rahhal, B., Heermann, S., Heidrich, S., Wiehle, M., Krieglstein, K., 2008. Transforming growth factor beta cooperates with persephin for dopaminergic phenotype induction. Stem Cells 26, 1683–1694.
Sacconi, S., Feasson, L., Antoine, J.C., Pecheux, C., Bernard, R., Cobo, A.M., Casarin, A., Salviati, L., Desnuelle, C., Urtizberea, A., 2012. A novel CRYAB mutation resulting in multisystemic disease. Neuromuscul. Disord.: NMD 22, 66–72.
Schaefer, M.H., Fontaine, J.F., Vinayagam, A., Porras, P., Wanker, E.E., Andrade-Navarro, M.A., 2012. HIPPIE: Integrating protein interaction networks with experiment based quality scores. PLoS One 7, e31826.
Sharma, B.K., Smith, C.C., Laing, J.M., Rucker, D.A., Burnett, J.W., Aurelian, L., 2006. Aberrant DNA methylation silences the novel heat shock protein H11 in melanoma but not benign melanocytic lesions. Dermatology 213, 192–199.
Sharp, P., Krishnan, M., Pullar, O., Navarrete, R., Wells, D., de Belleroche, J., 2006. Heat shock protein 27 rescues motor neurons following nerve injury and preserves muscle function. Exp. Neurol. 198, 511–518.
Shemetov, A.A., Seit-Nebi, A.S., Gusev, N.B., 2011. Phosphorylation of human small heat shock protein HspB8 (Hsp22) by ERK1 protein kinase. Mol. Cell. Biochem. 355, 47–55.
Smith, C.C., Li, B., Liu, J., Lee, K.S., Aurelian, L., 2011. The levels of H11/HSPB8 DNA methylation in human melanoma tissues and xenografts are a critical molecular marker for 5-Aza-2′-deoxycytidine therapy. Cancer Investig. 29, 383–395.
Sowa, G.A., Perera, S., Bechara, B., Agarwal, V., Boardman, J., Huang, W., Camacho-Soto, A., Vo, N., Kang, J., Weiner, D., 2014. Associations between serum biomarkers and pain and pain-related function in older adults with low back pain: a pilot study. J. Am. Geriatr. Soc. 62, 2047–2055.
Stelzl, U., Worm, U., Lalowski, M., Haenig, C., Brembeck, F.H., Goehler, H., Stroedicke, M., Zenkner, M., Schoenherr, A., Koeppen, S., Timm, J., Mintzlaff, S., Abraham, C., Bock, N., Kietzmann, S., Goedde, A., Toksoz, E., Droege, A., Krobitsch, S., Korn, B., Birchmeier, W., Lehrach, H., Wanker, E.E., 2005. A human protein-protein interaction network: a resource for annotating the proteome. Cell 122, 957–968.
Stuppia, G., Rizzo, F., Riboldi, G., Del Bo, R., Nizzardo, M., Simone, C., Comi, G.P., Bresolin, N., Corti, S., 2015. MFN2-related neuropathies: clinical features, molecular pathogenesis and therapeutic perspectives. J. Neurol. Sci. 356, 7–18.
Sugiyama, Y., Suzuki, A., Kishikawa, M., Akutsu, R., Hirose, T., Waye, M.M., Tsui, S.K., Yoshida, S., Ohno, S., 2000. Muscle develops a specific form of small heat shock protein complex composed of MKBP/HSPB2 and HSPB3 during myogenic differentiation. J. Biol. Chem. 275, 1095–1104.
Sun, Y., Mansour, M., Crack, J.A., Gass, G.L., MacRae, T.H., 2004. Oligomerization, chaperone activity, and nuclear localization of p26, a small heat shock protein from *Artemia franciscana*. J. Biol. Chem. 279, 39999–40006.
Tang, B.S., Zhao, G.H., Luo, W., Xia, K., Cai, F., Pan, Q., Zhang, R.X., Zhang, F.F., Liu, X.M., Chen, B., Zhang, C., Shen, L., Jiang, H., Long, Z.G., Dai, H.P., 2005. Small heat-shock protein 22 mutated in autosomal dominant Charcot-Marie-Tooth disease type 2L. Hum. Genet. 116, 222–224.
Tazir, M., Hamadouche, T., Nouioua, S., Mathis, S., Vallat, J.M., 2014. Hereditary motor and sensory neuropathies or Charcot-Marie-Tooth diseases: an update. J. Neurol. Sci. 347, 14–22.
Timmerman, V., De Jonghe, P., Simokovic, S., Lofgren, A., Beuten, J., Nelis, E., Ceuterick, C., Martin, J.J., Van Broeckhoven, C., 1996. Distal hereditary motor neuropathy type II (distal HMN II): mapping of a locus to chromosome 12q24. Hum. Mol. Genet. 5, 1065–1069.
von Maltzahn, J., Chang, N.C., Bentzinger, C.F., Rudnicki, M.A., 2012. Wnt signaling in myogenesis. Trends Cell Biol. 22, 602–609.
Wettstein, G., Bellaye, P.S., Micheau, O., Bonniaud, P., 2012. Small heat shock proteins and the cytoskeleton: an essential interplay for cell integrity? Int. J. Biochem. Cell Biol. 44, 1680–1686.
Xia, X., Zhou, H., Huang, Y., Xu, Z., 2006. Allele-specific RNAi selectively silences mutant SOD1 and achieves significant therapeutic benefit in vivo. Neurobiol. Dis. 23, 578–586.
Ylikallio, E., Konovalova, S., Dhungana, Y., Hilander, T., Junna, N., Partanen, J.V., Toppila, J.P., Auranen, M., Tyynismaa, H., 2015. Truncated HSPB1 causes axonal neuropathy and impairs tolerance to unfolded protein stress. BBA clinical 3, 233–242.